Fermi National Accelerator Laboratory

FERMILAB-Conf-92/378

Hyperon Polarization: An Experimental Overview

Joseph Lach

Fermi National Accelerator Laboratory
P.O. Box 500, Batavia, Illinois 60510

December 1992

Invited talk at the *International Workshop on Flavour and Spin in Hadronic and Electromagnetic Interactions*, Villa Guilino, Torino, Italy, September 21-23, 1992

Disclaimer

Hyperon Polarization: An Experimental Overview

Joseph Lach

Fermilab

Abstract

The fact that inclusively produced hyperons are produced with significant polarization was first discovered at Fermilab about seventeen years ago. This and subsequent experiments showed that Λ° were produced polarized while $\overline{\Lambda}^\circ$ had no polarization in the same kinematical region. This set the stage for many experiments which showed that most hyperons are produced polarized. Recent Fermilab experiments have showed that this phenomena is even more complex than previously thought and theoretical understanding is still lacking. Nevertheless polarized hyperon beams have been an extremely useful experimental tool in measuring hyperon magnetic moments and hyperon β-decay. Recently, hyperon radiative decays have been studied and magnetic moment precession of channeled particles in bent crystals has been observed.

My aim in this talk is to acquaint you with some of the rich phenomena in hyperon polarization. This is a field which has seen much experimental work in the last few years. It has also posed significant challenges to our theoretical understanding. Let me familiarize you with some of the basic properties of hyperons and some of the techniques that are used to study them.

The SU(3) combinations of the three lowest mass quarks (u, d, and s) to form baryons are depicted in Figure 1. Here I ignore, at

least for the time being, the three heavier quarks (c, b, and t). I make the normal definition of hypercharge as the sum of baryon number and strangeness. On the vertical scale I plot the hypercharge, Y, vs the third component of the isotopic spin. Identifying electric charge as one half the hypercharge plus the third component of isotopic spin, I form the baryon octet and decouplet. The lowest mass spin 1/2 baryons are identified in Figure 1 as well as the lowest mass spin 3/2 baryons.

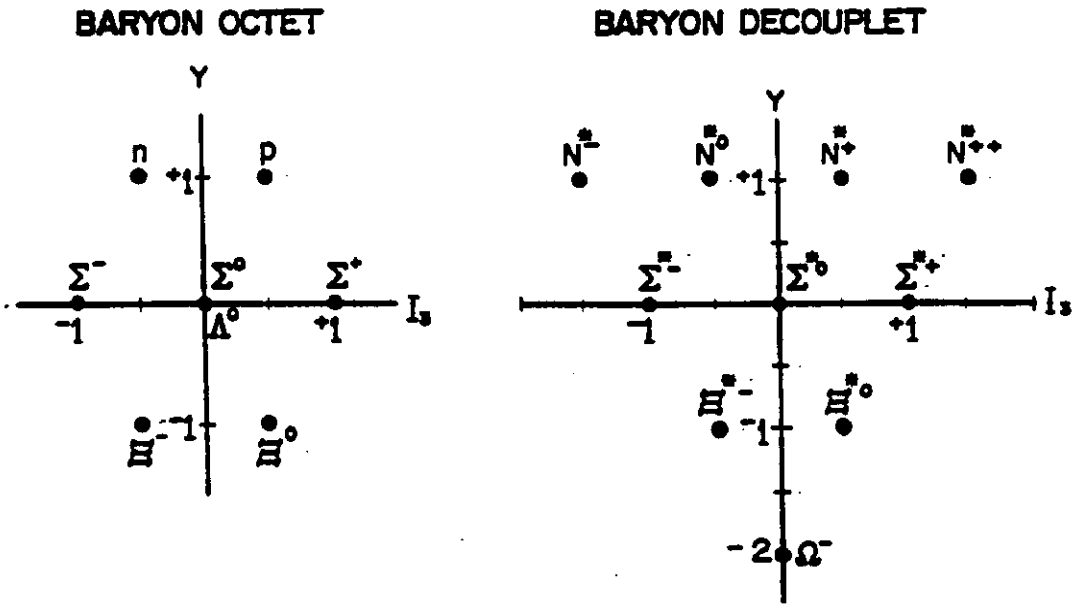

Figure 1.
The Quark Structure of the Baryons

Within the octet all of the members are stable under the strong interactions; the rest - except for the proton - decay by way of the weak interactions. The Σ° can also decay electromagnetically, $\Sigma^\circ \rightarrow \Lambda^\circ \gamma$; the proton is stable. Among the lowest mass members of the decouplet only the Ω^- does not decay strongly. Table 1 summarizes[1] the quark content and lifetimes of the long lived baryons; that is, those that do not have strong decays.

Table 1 The Long Lived Baryons

	Baryon	Quark Content	Mass MeV/c^2	Lifetime Sec
Octet				
	p	uud	938.27	stable
	n	udd	939.57	889
Hyperons	Λ°	uds	1115.63	2.632×10^{-10}
	Σ^+	uus	1189.37	7.99×10^{-11}
	Σ°	uds	1192.55	7.4×10^{-20}
	Σ^-	dds	1197.43	1.479×10^{-10}
	Ξ°	uss	1314.9	2.90×10^{-10}
	Ξ^-	dss	1321.32	1.639×10^{-10}
Decouplet				
	Ω^-	sss	1672.43	8.22×10^{-11}

Much of the early data on hyperon static properties such as lifetimes, decay modes, etc. was extracted from low energy bubble chamber photographs. Figure 2 is a bubble chamber photograph taken from the thesis of Gershwin[2]. It shows a photograph from the Lawrence Berkeley Laboratory 25 inch bubble chamber exposed to a 390 MeV/c K^- beam. The beam enters from the bottom of the picture and produces an interaction identified as

$$K^-p \rightarrow \Sigma^+\pi^-$$

One also sees the subsequent rare radiative decay, $\Sigma^+ \rightarrow p\gamma$, and the photon converting to an electron-positron pair near the top of the photograph. The short dark track is the Σ^+ and the longer connected dark track is the proton. The production dynamics of the hyperon is well known from the study of low energy phase shifts[3]. The energy of the K^- beam was chosen to have the center of mass energy near the mass of the $Y_0^*(1530)$. This D-wave resonance interferes with the S-wave background to produce Σ^+ with about 37% polarization. This is a very important technique to study the spin structure of the hyperons.

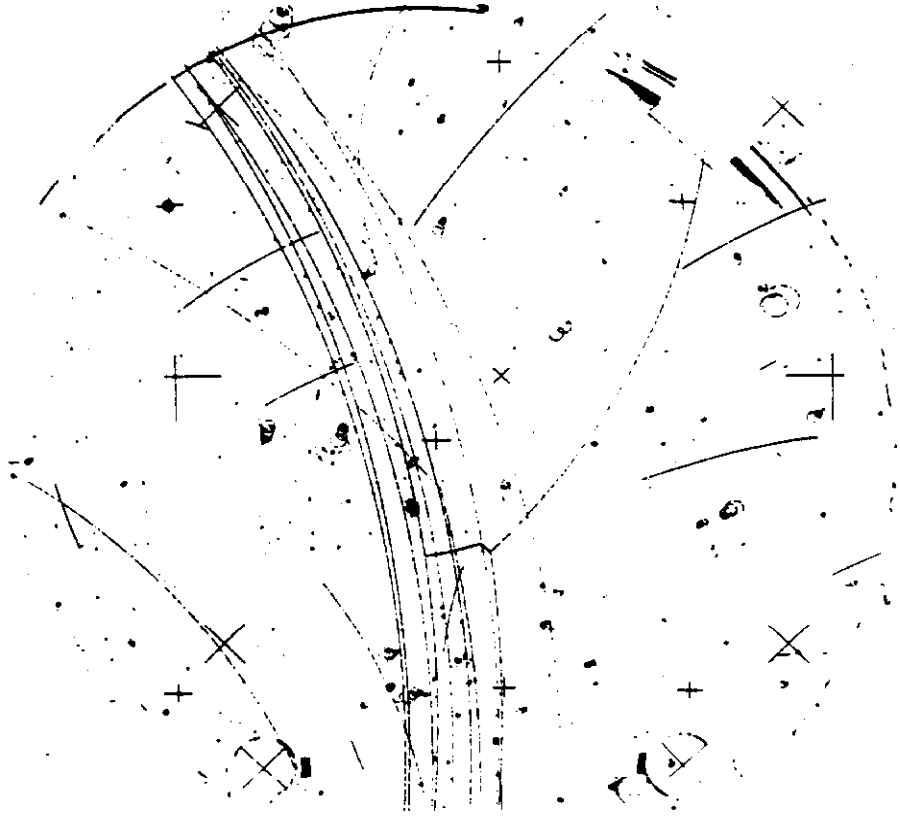

Figure 2
K^- interaction in LBL 25 inch bubble chamber showing
$K^-p \rightarrow \Sigma^+\pi^-$ and the subsequent decay $\Sigma^+ \rightarrow p\gamma$

The bubble chamber technique has serious drawbacks. One is its limitation to only a few tracks per picture, and the Σ^+ with its short path length does not curve appreciably in the magnetic fields available in bubble chambers. If the hyperons could be produced with decay lengths long enough to separate their production vertices from their decay positions then one would not be encumbered with the backgrounds of the production region. It is this fact which pushed the development of hyperon beams.

There are a number of reviews describing hyperon beams and the physics programs that have utilized them[4-7].

What are the essential elements of a hyperon beam?

*Start with a high energy proton beam
*Interact the beam in a small target to produce hyperons

*Select particles produced in the forward direction.

*Collimate in the other directions. Interact as many of the other secondary particles as practical, especially the pions before they can decay to muons.

*Magnetically select the desired momentum

*Do all of the above in as short a distance as possible to maximize the number of hyperons that survive. This puts a premium on

**high magnetic fields
**high resolution detectors
**high energy

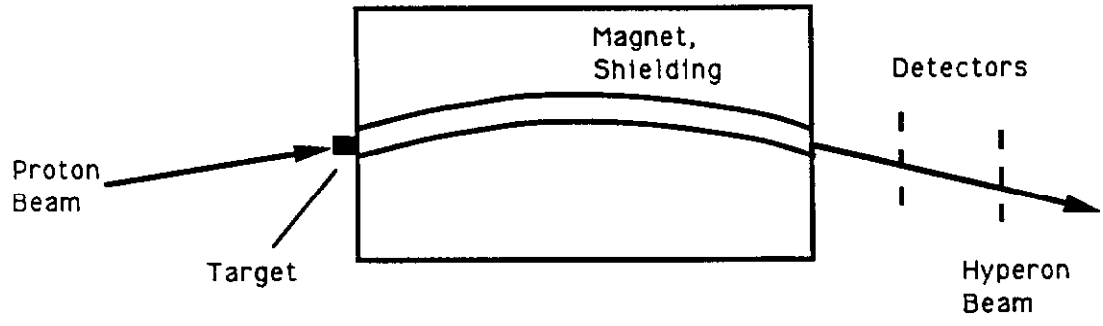

Figure 3
Essential Elements of a Charged Hyperon Beam

In Figure 3, we see the essential elements of a hyperon beam. The Fermilab hyperon beam in Proton Center has a 7m long magnet, the hyperon magnet[8], with a vertical magnetic field of about 3.5 T. The inner portion of the magnet containing the channel is removable and can be fitted with a curved channel appropriate for a charged beam or a straight channel for a neutral beam. A set of magnets upstream of the hyperon magnet allows for the angle of the proton beam impinging on the target to be varied either in the horizontal or vertical direction. This allows for the targeting angle to be varied between about $\approx\pm 5$ mrad in either plane for 800 GeV incident protons. The transverse momentum, p_t, of the produced beam particle is just the product of the sine of the targeting angle and the hyperon momentum. Along with the

Feynman x (x_F), it is used to characterize a hyperon beam. To a good approximation, x_F is just the ratio of the secondary particle momentum divided by the incident proton momentum. The ability to change the targeting angle in both the horizontal and vertical planes is important since it allows one to control the direction of the hyperon polarization as will be discussed later.

Following the hyperon magnet is a set of high resolution spatial detectors. In the earlier beams these were spark chambers and then proportional chambers; now silicon strip detectors are used. In a recent configuration[9], a Cu target of 0.5 mm full width in the horizontal plane coupled with 50 μm pitch silicon strip detectors resulted in momentum resolution of ≈0.2% ($\Delta p/p$) and angular resolution of ≈10 μrad.

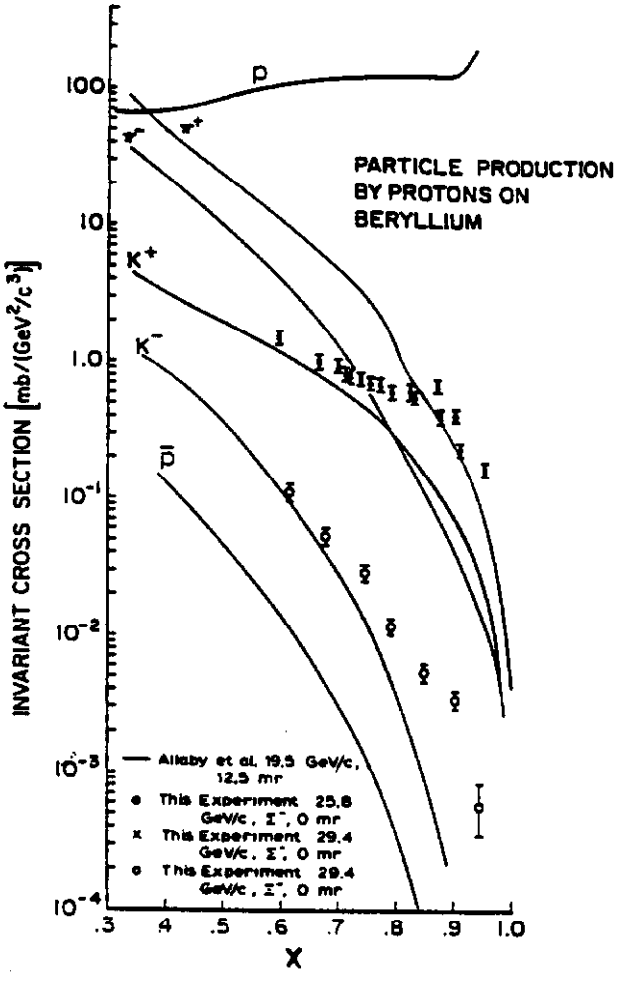

Figure 4
Hyperon Production Comparison
Cross section vs x_F

These early hyperon beams provided the first systematic measurements of hyperon fluxes and provided the "engineering" measurements for later beams. Figure 4 shows an early measurement[10] of these hyperon fluxes and a comparison with production of charged pions and kaons. This comparison is important since these are the contaminants to the hyperon beam and their numbers will usually limit rates in the apparatus designed to study hyperon properties.

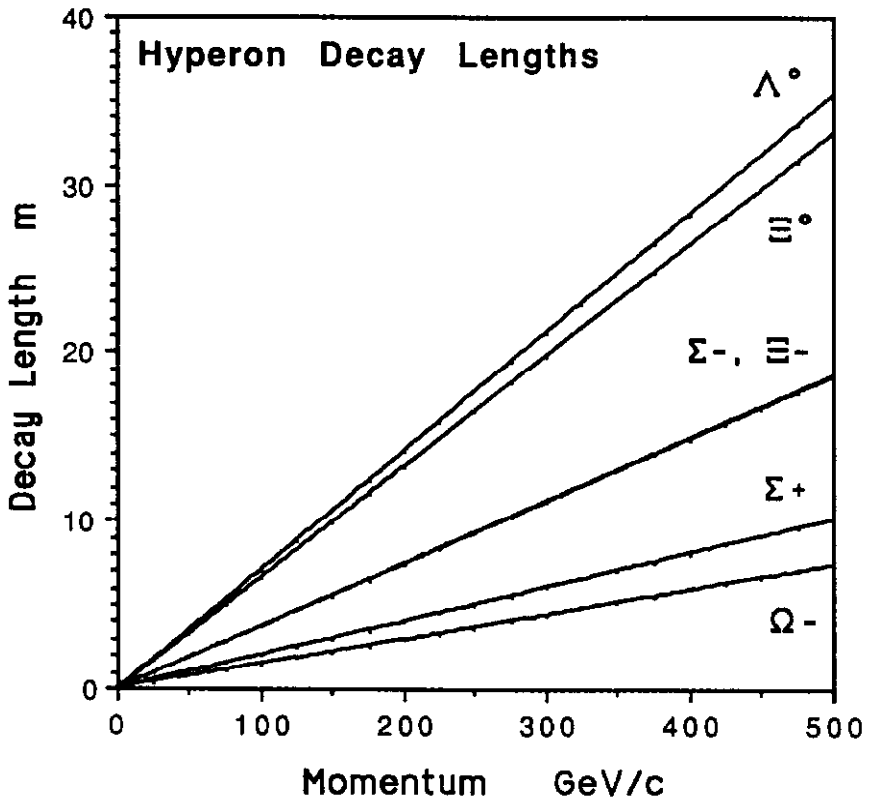

Figure 5
Hyperon decay lengths as a function of momentum

Figure 4 deserves some comments. Plotted is the measured production cross section as a function of x_F. These yields have been corrected for decay losses and extrapolated back to the production target. One notes a surprising fact: at large x_F the yield of Σ^- is greater than that of π^-, and that of Ξ^- is greater than that of K^-! This demonstrated that hyperons are produced

copiously at high energies and are ≈10% of all produced particles. It also showed the desirability of yet higher energy beams so that these high yields could be realized well downstream of the target. Figure 5 shows the hyperon decay lengths versus of their momenta.

Figure 6 is a diagram of the early CERN PS hyperon beam. That significant hyperon fluxes were available even at CERN PS energies[11] was beautifully demonstrated by the Cerenkov counter curve taken at the exit of their hyperon channel in Figure 6. The total distance from the target to the end of the Cerenkov counter was ≈4m.

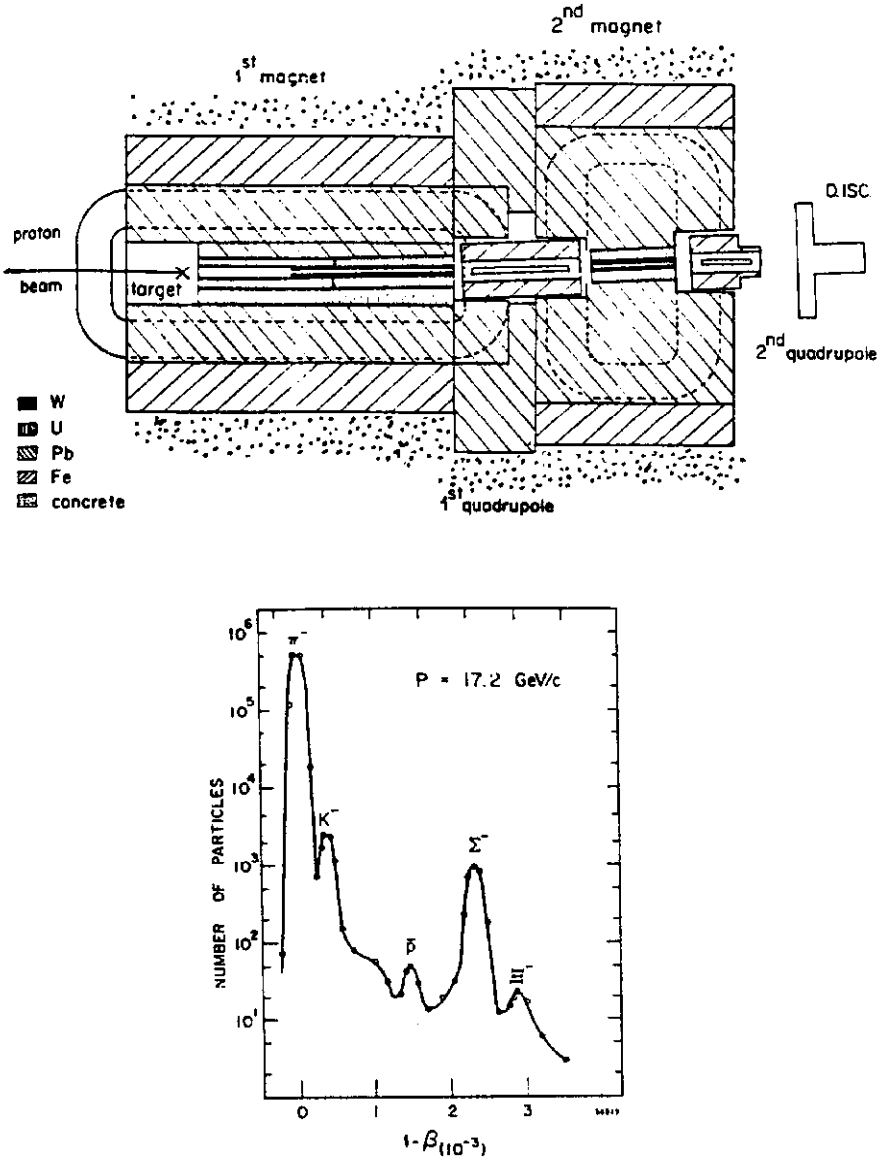

Figure 6

Hyperon beam diagram and velocity curve at 17.2 GeV/c showing the counting rate as a versus $1-\beta$

The hyperons of the octet shown in Figure 1 all have spin 1/2. Except for the Σ°, which decays electromagnetically, all have their major decays modes mediated by the weak interactions. Because these weak decays do not conserve parity, information from the distribution of their decay products can be used to determine their spin direction. I illustrate this in Figure 7 where I schematically represent the polarized decay of a $\Sigma^+ \to p\pi^\circ$. The center of mass distribution of the decay pion in this decay can be written as

$$I(\cos\theta) \approx 1 + \alpha P \cos\theta$$

where P is the Σ^+ polarization and α is characteristic of the weak decay properties of the particle.

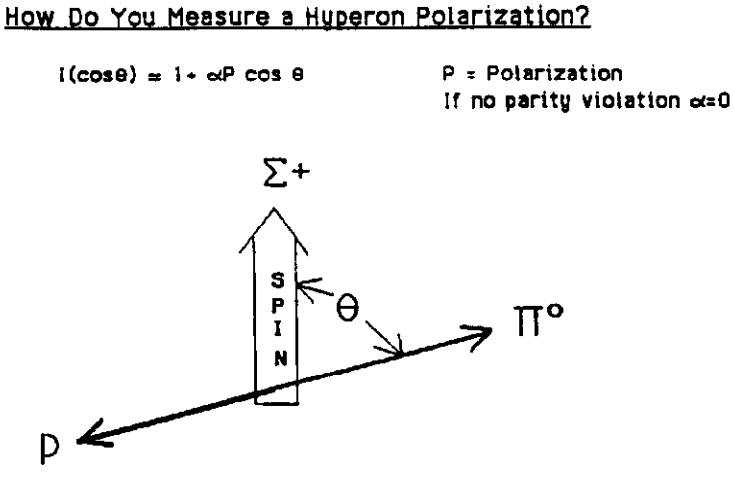

Figure 7
Decay of a polarized $\Sigma^+ \to p\pi^\circ$.

The physics of the decay is contained in α. If we just wish to measure a polarization or see the spin direction precess by a magnetic field we need not be concerned how nature gave us α; we can just use it. Note that we measure asymmetries, $A=\alpha P$, the product of α and P. We need to have them both non zero to measure a spin direction. Naturally, the larger the value of α, the easier it is to measure A and hence the polarization.

Table 2 is a list[1] of some of the more important hyperon decay modes, branching ratios, and α parameters for these decays. From Table 2 we see that α for the various decay modes can assume a wide range of values. The decay $\Sigma^+ \to p\pi^\circ$ has α near its maximum negative value, making it easy to measure the Σ^+ polarization

through this decay mode. The decay $\Sigma^- \to n\pi^-$ has a small but clearly non-zero value of α making it necessary to have a large data sample and good control of systematic errors to get a measurement of its polarization.

In decays such as $\Xi^- \to \Lambda^\circ\pi^-$, where one also observes the subsequent decay, $\Lambda^\circ \to p\pi^-$, information about the spin direction of the Ξ^- is also contained in the decay distribution[5] of the decaying Λ°.

Table 2 Hyperon Decay Properties

Decay Mode	BR %	α
$\Sigma^+ \to p\pi^\circ$	51.6	-0.980±0.019
$\Sigma^+ \to n\pi^+$	48.3	0.068±0.013
$\Sigma^- \to n\pi^-$	99.8	-0.068±0.008
$\Sigma^- \to ne^-\bar{\upsilon}$	0.1	-0.519±0.104
$\Lambda^\circ \to p\pi^-$	64.1	0.642±0.013
$\Lambda^\circ \to n\pi^+$	35.7	0.65±0.05
$\Xi^\circ \to \Lambda^\circ\pi^\circ$	100.	-0.411±0.022
$\Xi^- \to \Lambda^\circ\pi^-$	100.	-0.456±0.014
$\Omega^- \to \Lambda^\circ K^-$	67.8	-0.026±0.026
$\Omega^- \to \Xi^\circ\pi^-$	23.7	0.09±0.14
$\Omega^- \to \Xi^-\pi^\circ$	8.6	0.05±0.21

From Table 2, we see that for Ω^- decays, the values of α are all small and consistent with zero. In this case we must use the information from the subsequent Λ° decay to determine the parent polarization. Note that one can still measure the α parameters for the Ω^- decay even if the Ω^- is not polarized[7]. This is further complicated by the fact that the Ω^- has spin =3/2. However, similar procedures as for the Ξ^- decay have been developed[12].

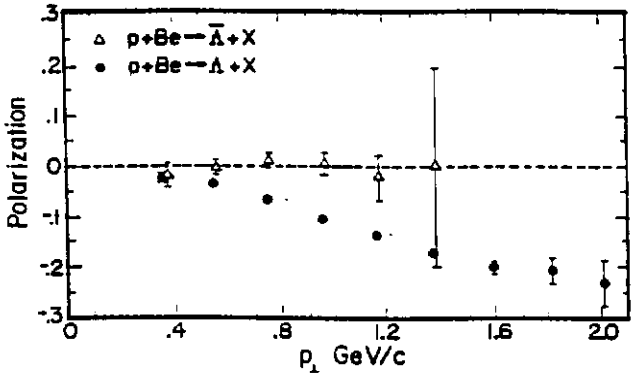

Figure 8
Polarizations of Λ° and $\bar{\Lambda}^\circ$

Significant Λ° polarization was measured in the early Fermilab neutral hyperon beam[13]. Figure 8 shows data[14] for Λ° and $\bar{\Lambda}^\circ$ produced by 400 GeV protons. The polarization is plotted as a function of the transverse momentum, p_t, of the produced hyperon relative to the incident proton momentum. The Λ° polarization was found to be zero in the forward direction (as required by rotational symmetry for production from an unpolarized beam and target) and decreased linearly to $\approx$-25% at a transverse momentum (p_t) of $\approx$1.0 GeV/c. These experiments also showed that the polarization had little dependence on the initial energy of the proton or the target material. We use the conventional sign definition[15] for the inclusive hyperon polarization: a positive polarization is in the same direction as the cross product of the incident beam direction with the produced hyperon direction.

It must be kept in mind that these are inclusive measurements and we only measure one of the reaction products. We do not know if the Λ° was produced directly as a Λ° or was produced as a Σ° which then decayed $\Sigma^\circ \rightarrow \Lambda^\circ \gamma$. For that matter we do not know if the Λ° (or Σ°) was produced as a Y^* resonance which decayed strongly to the Λ° (or Σ°).

What about the p_t and x_F dependence of the polarization? Figure 9 shows[16] the Λ° polarization at two different values of x_F. Note that it has a linear increase with p_t and then seems to plateau. The level of the plateau region is a function of x_F. QCD predicts[17] that at large values of p_t the polarization should vanish but does not give us any quantitative measure of what this value is.

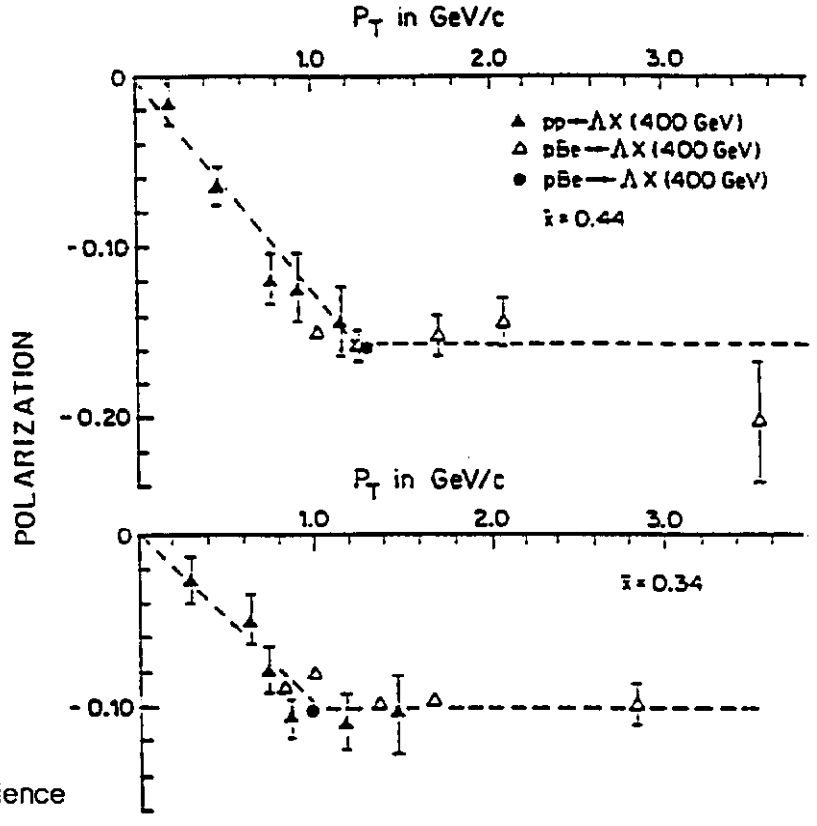

Figure 9
p_t and x_F dependence of Λ° polarization

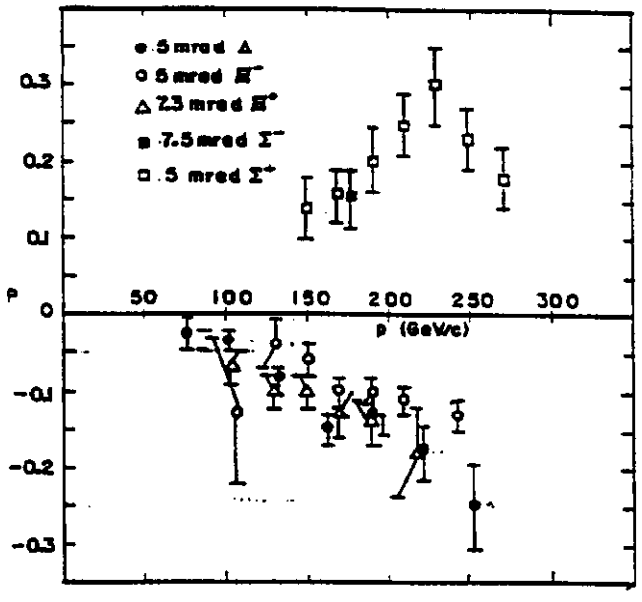

Figure 10
Polarization of other hyperons. Plotted is the polarization vs hyperon momentum at fixed angles. The horizontal axis is thus proportional p_t.

The clear evidence (Figure 8) that Λ° are produced with significant polarization came as a surprise. The empirical conjecture that the more quarks incorporated from the sea reduces the produced hyperon polarization seemed to be confirmed by measurements of the polarization[12,18-25] of $\Sigma^\pm$, Ξ^-, and Ω^- hyperons. Figure 10 shows the measured polarizations of some other hyperons. Plotted here is the polarization as a function of the hyperon momentum at a fixed production angle. Since $p_t = P_h \sin\theta$, where P_h is the hyperon momentum and θ the production angle, the horizontal axis is proportional to p_t. These are all produced by 400 GeV protons. Significant polarizations seem to be a general property of hyperon production at high energies.

Can one see any pattern to these polarizations? Perhaps some clues may become evident if we look at the spin structure of the final state hyperons. We examine the SU(6) quark spin wave functions of the baryons taken from any modern text or the early paper of Franklin[26]. We note that in the Λ° wave function, since the u and d quarks are in a singlet state, the spin of the Λ° is the spin direction of the s quark. The spin states of the Σ's are all triplets. Heller[14] pointed out that by assuming that the produced s quark carries the polarization, one could infer that the polarization of the Σ^+ and the Σ° should be opposite in sign and 1/3 of the Λ° polarization. The sign is indeed opposite but the factor of 1/3 does not seem to hold (is the Λ° produced as Λ° or Σ° or Y^* states?).

These polarizations have generally been attributed to peripheral mechanisms in which some of the proton valence quarks assimilate a strange quark from the sea to form a polarized hyperon. We can take hyperon wave functions and write the valence quark diagrams shown in Figure 11. I have separated them into three rows corresponding to whether the produced hyperon (or antihyperon) retains one, two or zero of the projectile's valence quarks. In our notation for the antiparticles, we adopt the convention that the written sign is the electrical charge of the particle under consideration. Thus, for the positively charged antiparticle of the Ξ^- we write $\overline{\Xi}^+$, not $\overline{\Xi}^-$.

In Figure 11, using the SU(6) wave functions, I have noted the spin configurations of the hyperons and the measured polarization directions of the produced hyperons. If one ignores the

antihyperons, one notes that the s quark is always produced with its spin down. In these interactions, the Λ° is a leading particle and the $\overline{\Lambda}^\circ$ is not. Might this be significant? One sees each of the hyperons being produced with polarization of $\approx$10-20% at $p_t \approx 1$ GeV/c. The fact that early experiments had shown $\overline{\Lambda}^\circ$ to be unpolarized, where in the same kinematic range Λ° was polarized, lent credence to the idea that polarization is a leading particle effect. This was supported by measurements[12] showing the Ω^- to be unpolarized in this same kinematical region. Since the Ω^- is composed of three strange valence quarks it contains none of the valence quarks of the incident proton.

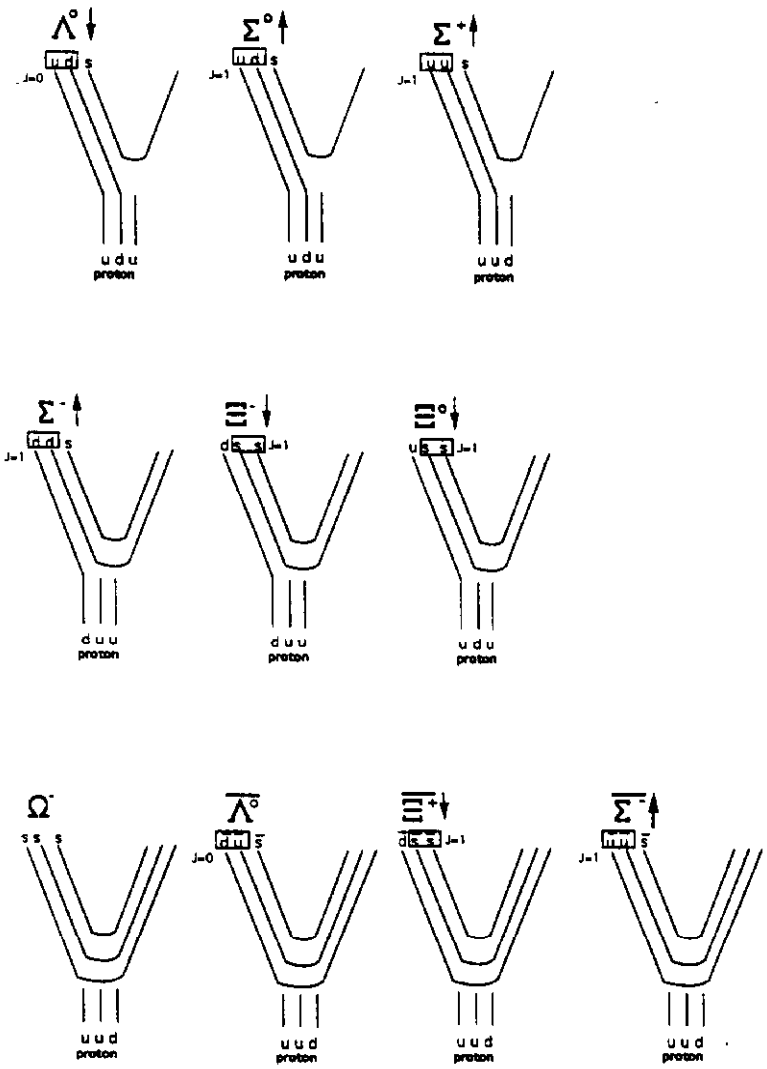

Figure 11.
Hyperon Polarization Diagrams

However, recent data have cast great doubt on this picture. Measurement of the $\overline{\Xi}^+$ polarization by the Fermilab E756 group[27], shown in Figure 12, shows $\overline{\Xi}^+$ to be polarized by about the same amount as the Ξ^-.

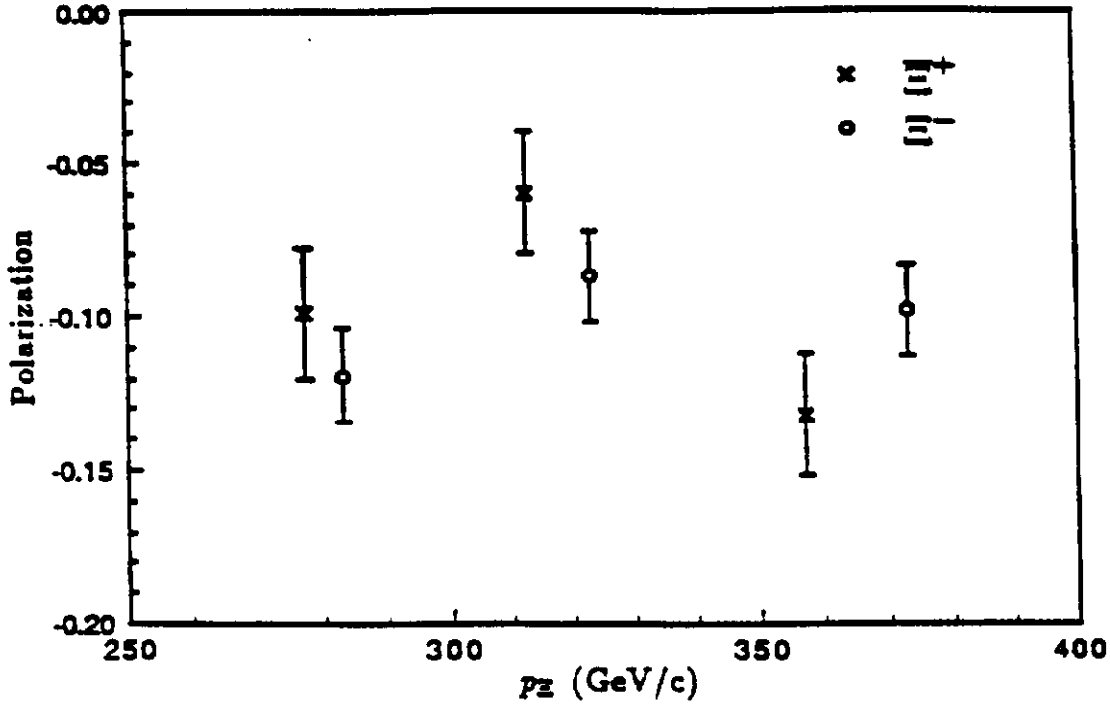

Figure 12.
Ξ^- and $\overline{\Xi}^+$ polarization

Our E761 group has measured the polarization of 375 GeV/c Σ^+ and $\overline{\Sigma}^-$ produced by 800 GeV protons on a Cu target. The Σ^+ was detected via its decay $\Sigma^+ \to p\pi^\circ$ and the $\overline{\Sigma}^-$ through its charge conjugate decay $\overline{\Sigma}^- \to \overline{p}\,\pi^\circ$. Figure 13ab shows the reconstructed π° mass squared for the negative and positive beam. I show this to illustrate the capabilities of modern hyperon beams in statistics and resolution. In the positive data, one clearly sees the rare radiative decay, $\Sigma^+ \to p\gamma$, whose study was the goal of this experiment. Both this decay and the charge kaon decays are visible but can be easily removed by making a selection on the missing mass.

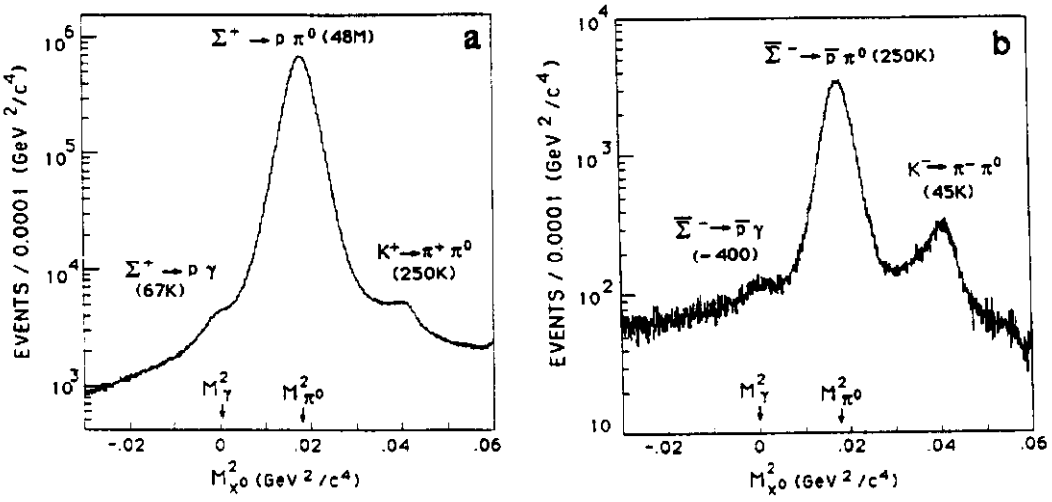

Figure 13
Event distributions of the mass squared of the missing neutral particle (X°) for the hypothesis $\Sigma^+ \to pX^\circ$ for positive and negative beam candidates

Figure 14 shows the measured polarizations of Σ^+ and $\overline{\Sigma}^-$ as a function of p_t. In this **preliminary** data one sees that the $\overline{\Sigma}^-$ is also produced with $\approx$7% polarization near $p_t \approx 1$ GeV/c. A Be target was used in the E756 $\overline{\Xi}^+$ data and a Cu target in E761. However, the nature of the target material does not seem to have a major effect on hyperon production. Pondrom[5] has a good summary of target material dependence of hyperon production and polarization data.

This Σ^+ data shows that the polarization increases with p_t, goes through a maximum near p_t = 1 GeV/c and then decreases. This is the first time this decrease has been observed in a high energy hyperon polarization.

The data of Figure 14 show points taken with both horizontal and vertical targeting for Σ^+ and $\overline{\Sigma}^-$. In horizontal targeting, the incident beam direction is changed in the horizontal (H) plane producing polarization in the same plane (vertical) as the magnetic field of the hyperon magnet Thus there is no spin rotation as the hyperons traverse the magnet. Targeting in the vertical (V) plane produces a polarization in the horizontal plane, perpendicular to

the magnet field, thus producing maximum spin rotation as would be desired for measurement of a magnetic moment.

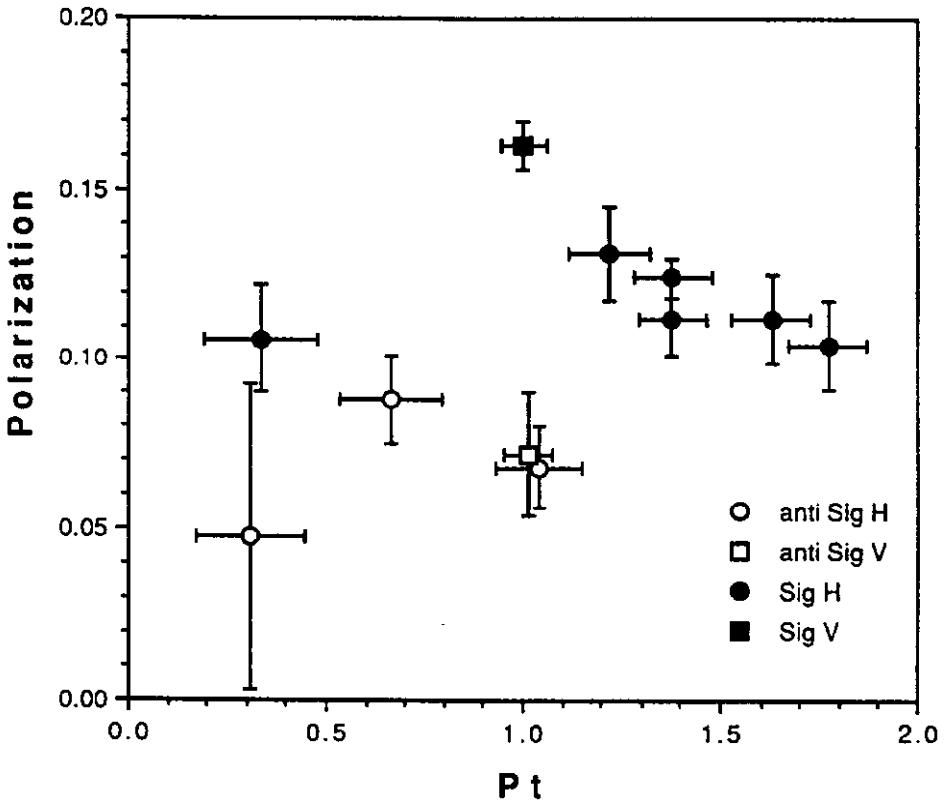

Figure 14

Σ^+ and $\overline{\Sigma}^-$ polarization as a function of Pt

Among the many proposed models[28-31], let me mention two approaches to the polarization question - both involving similar leading particle effects. One is that of the Lund group[32] whose model assumes $q\overline{q}$ pairs are produced from the sea via the breaking of a QCD string but conserving local angular momentum. DeGrand and Miettinen[33] propose two simple rules: quarks which gain longitudinal momentum combine with spins down; quarks which lose longitudinal momentum combine with spins up. This is equivalent to a Thomas precession and a spin orbit coupling. Both models explain much of the hyperon data. The magnitudes of some of the polarizations are at odds with each of the models. None of them can explain the polarizations of the antihyperons. Other models are discussed in a review by P. Kroll[34] and is

recommended although it was done before the polarizations of the $\bar{\Xi}^+$ and $\bar{\Sigma}^-$ were measured.

Clearly the $\Lambda^\circ/\bar{\Lambda}^\circ$, $\Xi^-/\bar{\Xi}^+$, and $\Sigma^+/\bar{\Sigma}^-$ systems exhibit a rich and challenging set of polarization phenomena that cry out for insightful ideas.

Even though one may not be able to understand the underlying mechanism for hyperon polarization phenomena, one can use it as a tool for other physics measurements.

The fact that hyperons can be produced with significant polarization has allowed us to measure hyperon magnetic moments to remarkable precision. As I previously discussed one can control the hyperon polarization direction by the targeting angle of the incident proton beam. With this control one can produce the polarization perpendicular to the magnetic field direction so that significant spin rotation occurs as it passes through the hyperon targeting magnet (Figure 3). For the case of Σ^+ in E761, our most recent experiment, we have a precession of the spin direction of

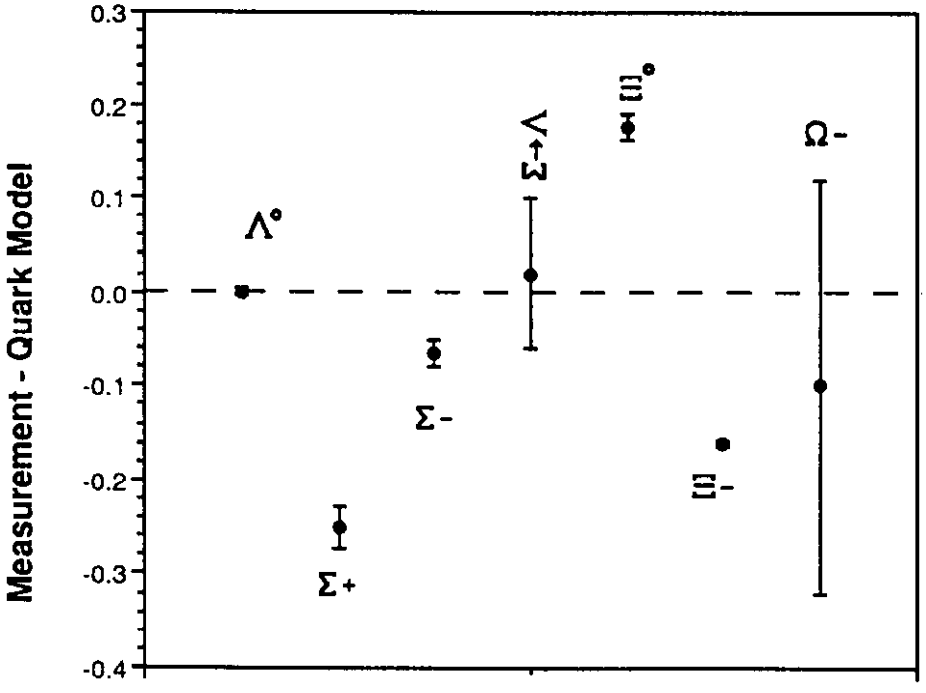

Figure 15.
Comparison between measured and Quark model predicted magnetic moments in nuclear magnetons

about 600°. This is not a small effect! The measurements[35] of the baryon magnetic moments has developed into a small industry.

I show in Figure 15 the comparison of the baryon magnetic moments with the naive quark model. In the naive quark model we assume simple SU(6) wave functions and that only the valence quarks contribute to the baryon magnetic moments Besides the magnetic moments, Figure 15 also includes the measurement of the $\Sigma^0 \rightarrow \Lambda^0 \gamma$ transition moment. The rate of this purely electromagnetic decay is also predicted by the same formalism.

The measurements have become increasingly more precise. Data exist from Fermilab E761 to improve the Σ^+ magnetic moment yet further and Fermilab E800 has an improved measurement of the Ω^- magnetic moment. These data continue to challenge model builders.

Studies of the β-decay of hyperons have provided crucial tests of the Cabibbo theory of weak interactions. Polarized hyperon beams have provided an ideal tool to study the spin structure of these decays. These techniques[36] are illustrated by Fermilab E715 which has made the definitive study of the decay $\Sigma^- \rightarrow n e^- \overline{\nu}$.

Hyperon radiative decays, illustrated by the decay $\Sigma^+ \rightarrow p\gamma$, have also been studied with high energy hyperon beams. These kinematically simple two body decays involve the interplay of weak, electromagnetic, and strong interactions. Only two experimental parameters characterize each of these decays: their branching ratio and the asymmetry parameter from the decay of the polarized hyperon. Recently Fermilab E761 has published[9] a precision measurement of the α parameter for the $\Sigma^+ \rightarrow p\gamma$ decay.

Let me conclude with a discussion of crystal channeling. The phenomenon of crystal channeling[37,38] has been of interest because of the very high effective magnetic fields that are involved. Figure 16 illustrates this phenomenon. Figure 16 depicts a crystal oriented so that a charged beam enters almost parallel to the crystal axis. A positively charged particle entering thus finds itself in a potential well formed by the positively charged arrays of nuclei. It is trapped -channeled- in this potential if the incident angle is near the crystal plane. If the angle is too large

it passes through the crystal without being channeled as indicated in the same figure.

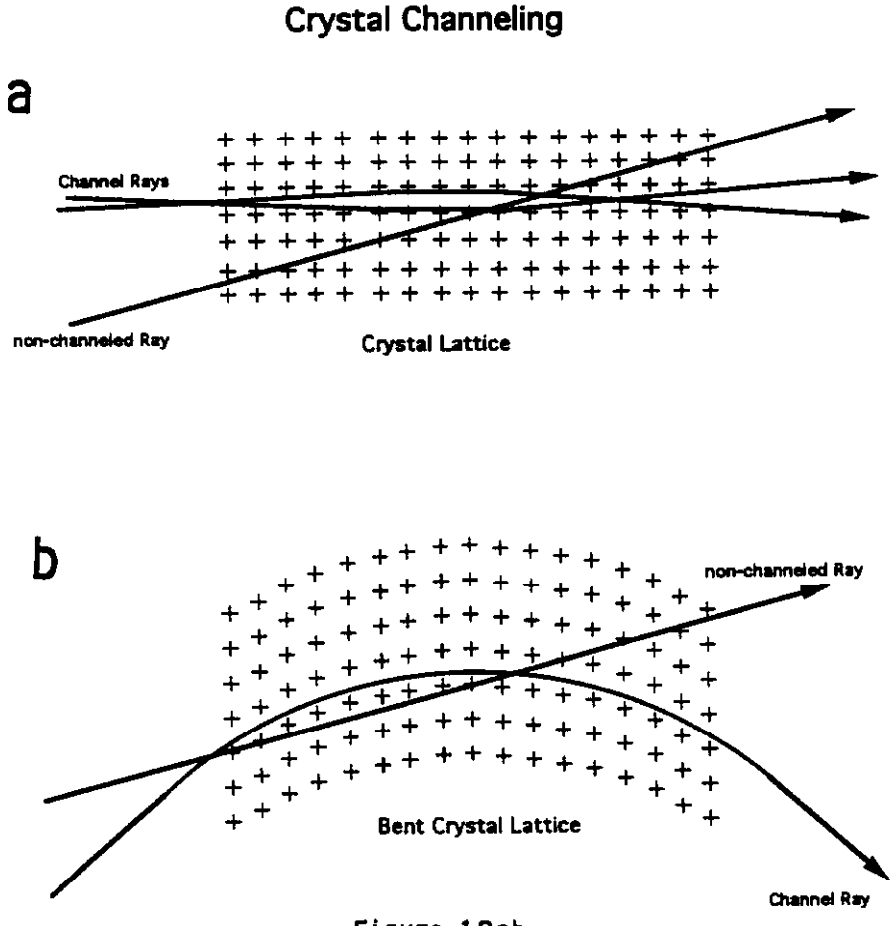

Figure 16ab
Channeling in straight and bent crystal

If one now bends the crystal as depicted in Figure 16b, one finds that one also bends the channeled beam[37]. From the momentum of the particle and the bend angle one realizes that the effective magnetic fields inside the crystal can be very large. Can these same large fields be used to precess the spin direction of a polarized beam? Fermilab E761, whose main goal was to look at hyperon radiative decays ($\Sigma^+ \to p\gamma$ and $\Xi^- \to \Sigma^-\gamma$), attempted to see this effect in a subsidiary experiment. A beam containing Σ^+ hyperons is a good candidate for investigating this effect since they can be produced polarized and have a large decay asymmetry parameter ($\alpha = -0.98$) for the common decay mode, $\Sigma^+ \to p\pi^\circ$. Hence,

one can readily measure their spin direction from the decay distribution.

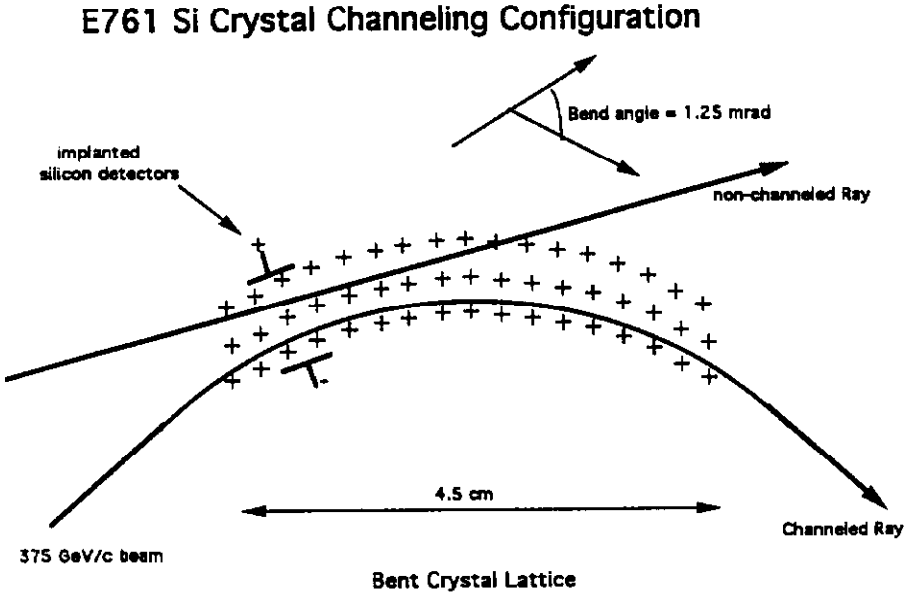

Figure 17
crystal setup for channeling

Figure 17 schematically shows the crystal configuration used in E761. A single crystal of silicon was placed in a 375 GeV/c beam which contained about 1% Σ^+ (the rest being mainly protons and π^+). This crystal was also implanted with solid state energy loss detectors so that the energy deposited in the crystal could be measured for each incident particle. Apparatus upstream (not shown) of the crystal measured the incident particle momentum and angle (with a precision of $\approx$0.2% and $\approx$ 10μrad respectively). A downstream spectrometer (also not shown) measured the particle momentum and trajectory a second time. Figure 18 shows some results[39] where no distinction is made between particle types. Thus it contains mostly protons and π^+. Figure 18b shows the difference between the angle measured entering and exiting the crystal. One sees a peak at about 1.65 mrad which is the known bending angle of the crystal.

Another characteristic is that the channeled particles lose less energy due to ionization than their non-channeled counterparts. Figure 18a shows the energy deposition in the crystal for those events which triggered[39] the apparatus The peak at lower energy loss values is due to channeled particles. The

solid line through the non channeled portion is a theoretical Landau distribution.

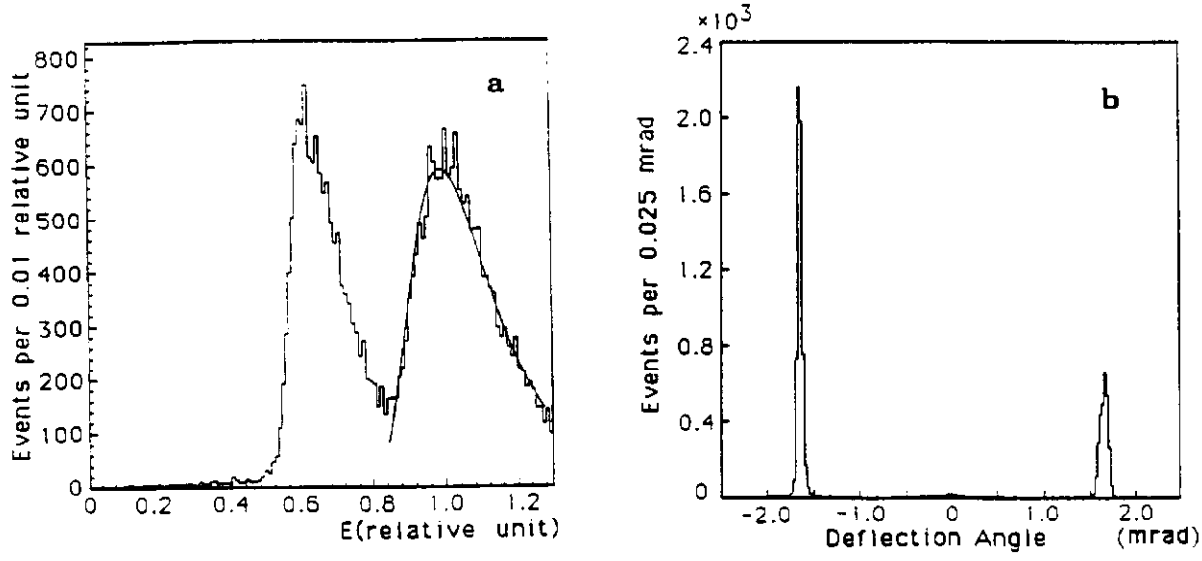

Figure 18
Crystal Channeling Data.
(a) Energy loss for non-channeled particles.
(b) Deflection of beam by crystal.

In this experiment the spin precession of channeled particles in bent crystals has been observed[39] for the first time. These crystals provided an effective magnetic field of 45 T which resulted in a measured spin precession of 60±17°. This agrees with the prediction of 62±2° using the world average[1] of Σ^+ magnetic moment measurements. This new technique gives a Σ^+ magnetic moment of 2.40±0.46±0.40 μ_N where the quoted uncertainties are statistical and systematic respectively. No evidence of depolarization is seen in the channeling process.

The crystal bend angle of 1.65 mrad was chosen to match the acceptance of the downstream spectrometer. The crystal was bent to angles as large as 10 mrad (without breaking!) which would correspond to an effective magnetic field of ≈275 T.

An exciting possibility is the application of this technique to charmed baryons which have a much shorter lifetime[1] than Σ^+. Note

that at 500 GeV/c the Λ^+_c and Ξ^+_c would have decay lengths of 1.18 and 2.64 cm respectively.

The phenomena of hyperon polarization in high energy interactions has forced us to rethink the basic physics of these processes. It has also provided us with a new tool which has been extremely useful in probing other fundamental processes.

I wishes to thank my colleagues on E761 for many discussions. This work is supported in part by the U.S. Department of Energy under contracts DE-AC02-76CH03000.

References

1. Particle data Group Phys. Rev. **D45**, 1 (1992).
2. L.K. Gershwin, PhD Thesis, UCRL-19246, U. ofCalifornia, Berkeley ,1969 (unpublished).
3. E. Segre,Nuclei and Particles (W. A. Benjamin, Inc., 1965).
4. J. Lach and L. Pondrom Annu. Rev. Nucl. Part. Sci. **29**, 203 (1979).
5. L. Pondrom Phys. Rep. **122**, 57 (1985).
6. J.M. Gaillard and G. Savage Ann. Rev. Nucl. Part. Sci. **34**, 351 (1984).
7. M. Bourquin and J.P. Repellin Phys. Reports **114**, 100 (1984).
8. T.R. Cardello *et al.*, Phys. Rev. **32**, 1 (1985).
9. M. Foucher *et al.*, Phys. Rev. Lett. **68**, 3004 (1992).
10. V. Hungerbuhler *et al.*, Phys. Rev. **D12**, 1203 (1975).
11. J. Badier *et al.*, Phys. Lett. **39B**, 414 (1972).
12. K.B. Luk *et al.*, Phys. Rev **D38**, 19 (1988).
13. G. Bunce Phys. Rev. **D18**, 3115 (1976).
14. K. Heller *et al.*, Phys. Rev. Lett. **41**, 607 (1978).
15. Basel Convention Helv. Phys. Act. Suppl. **VI**, (1961).
16. K. Heller, Proceedings of the 9th International Symposium on High Energy Spin Physics, Bonn, Germany, p 97, Springer-Verlag (1990).
17. G.L. Kane *et al.*, Phys. Rev. Lett. **41**, 1689 (1978).
18. C. Ankenbrandt *et al.*, Phys. Rev. Lett. **51**, 863 (1983).
19. C. Wilkinson *et al.*, Phys. Rev. Lett. **58**, 855 (1987).
20. Y.W. Wah *et al.*, Phys. Rev. Lett. **55**, 2551 (1985).
21. L. Deck *et al.*, Phys. Rev. **28**, 1 (1983).
22. G. Zapalac *et al.*, Phys. Rev. Lett **57**, 1526 (1986).

23. R. Rameika *et al.*, Phys. Rev. **D33**, 3172 (1986).
24. L.H. Trost *et al.*, Phys. Rev. **D40**, 1703 (1989).
25. H.T. Diehl *et al.*, Phys. Rev. Lett. **67**, 804 (1991).
26. J. Franklin Phys. Rev. **172**, 1807 (1968).
27. P.M. Ho *et al.*, Phys. Rev. Lett. **65**, 1713 (1990).
28. J. Szwed Phys. Lett. **105B**, 403 (1981).
29. P. Cea *et al.*, Phys. Lett. **209B**, 333 (1988).
30. J. Soffer and N.A. Tornqvist Phys. Rev. Lett. **68**, 907 (1992).
31. W.G.D. Dharmaratna and G.R. Goldstein Phys. Rev. **41**, 1731 (1990).
32. B. Andersson *et al.*, Phys. Lett. **85B**, 417 (1979).
33. T.A. DeGrand and H.I. Miettinen Phys. Rev. **24**, 2419 (1981).
34. P. Kroll, High Energy Spin Physics, Minneapolis, Minnesota, p 48, American Institute of Physics Conference Proceedings No. 187 (988).
35. J. Lach, Proceedings of the 9th International Symposium on High Energy Spin Physics, Bonn, Germany, p 87, Springer-Verlag (1990).
36. S.Y. Hsueh *et al.*, Phys. Rev. **D38**, 2056 (1988).
37. J.S. Forster *et al.*, Nucl. Phys. **B318**, 301 (1989).
38. R. Carrigan and J.A. Ellison. Relativistic Channeling (Plenun Press, New York, 1987).
39. D. Chen *et al.*, Phys. Rev. Lett. **69**, 3286 (1992).